

## Effects of Albedo on the MIR Emissivity Spectra of Silicates for Lunar Comparison



### Key Points:

- Space weathering affects midinfrared data from the Moon largely by altering regolith albedo
- Albedo affects the position of the Christiansen feature (CF) of minerals in the midinfrared under ambient and simulated lunar environment conditions
- Correlation between albedo and CF is shown in remote sensing data and laboratory experiments

### Supporting Information:

Supporting Information may be found in the online version of this article.

### Correspondence to:

K. A. Shirley,  
katherine.shirley@physics.ox.ac.uk

### Citation:

Shirley, K. A., Glotch, T. D., Donaldson, O., Trelewicz, J., Yang, Y., & Zhang, H. (2023). Effects of albedo on the MIR emissivity spectra of silicates for lunar comparison. *Journal of Geophysical Research: Planets*, 128, e2022JE007629. <https://doi.org/10.1029/2022JE007629>

Received 21 OCT 2022

Accepted 1 FEB 2023

### Author Contributions:

**Conceptualization:** K. A. Shirley, T. D. Glotch

**Formal analysis:** K. A. Shirley, O. Donaldson

**Funding acquisition:** T. D. Glotch

**Investigation:** K. A. Shirley

**Methodology:** K. A. Shirley, O.

Donaldson, J. Trelewicz

**Resources:** T. D. Glotch, J. Trelewicz, Y.

Yang, H. Zhang

**Writing – original draft:** K. A. Shirley

**Writing – review & editing:** T. D.

Glotch, Y. Yang, H. Zhang

K. A. Shirley<sup>1</sup> , T. D. Glotch<sup>2</sup> , O. Donaldson<sup>3</sup>, J. Trelewicz<sup>3</sup>, Y. Yang<sup>4</sup> , and H. Zhang<sup>5,6</sup> 

<sup>1</sup>Atmospheric, Oceanic, and Planetary Physics, University of Oxford, Oxford, UK, <sup>2</sup>Department of Geosciences, Stony Brook University, Stony Brook, NY, USA, <sup>3</sup>Department of Materials Science and Chemical Engineering, Stony Brook University, Stony Brook, NY, USA, <sup>4</sup>State Key Laboratory of Space Weather, National Space Science Center, Chinese Academy of Science, Beijing, China, <sup>5</sup>School of Earth Sciences, Planetary Science Institute, China University of Geosciences, Wuhan, China, <sup>6</sup>Key Laboratory of Spectral Imaging Technology, Xi'an Institute of Optics and Precision Mechanics, Chinese Academy of Sciences, Xi'an, China

**Abstract** We used laboratory analysis to investigate the effect of mineral albedo, as defined at 750 nm, on the midinfrared emissivity spectra of silicates under lunar environment conditions. Optical darkening has long been recognized as an effect of space weathering on the visible-to-near-infrared spectra of the Moon. However, space weathering has not been as thoroughly investigated in the mid-infrared. Because mid-infrared spectra are strongly influenced by the anisothermality of the lunar surface environment, it is likely that any darkening effects of space weathering would also change the thermal gradient in heavily space weathered lunar regolith. To isolate this variable, we added nanophase carbon to particulate samples of forsterite, augite, and anorthite to achieve a range of albedo samples and measured their midinfrared spectra under lunar environment conditions within the Planetary and Asteroid Regolith Spectroscopy Environment Chamber at Stony Brook University. We observe a shift in the Christiansen Feature maximum to longer wavelengths and decreasing spectral contrast with decreasing albedo. These shifts are well correlated with the observation of space weathering effects on the Diviner Lunar Radiometer Experiment compositional data, and point to the need for further investigation into the effects of space weathering on the midinfrared spectra of airless bodies.

**Plain Language Summary** Space weathering is a major process on the Moon that matures lunar soils over time. In this work, we try to isolate one of the effects of space weathering, darkening, to determine its effects on our interpretation of midinfrared emissivity spectra. We do so by adding nano-scale carbon particles to three silicate minerals and examine how the spectral features change as the sample gets darker under both ambient and simulated lunar environment conditions. We observe a decrease in overall spectral contrast and a shift in the Christiansen Feature (CF) position to longer wavelengths with increasing carbon content. This correlation between the darkening sample and CF value is similarly observed in the remote sensing data from Diviner Lunar Radiometer Experiment and Kaguya Multiband Imager instruments, demonstrating that it is an important factor to consider to accurately interpret composition from mid-infrared data of space weathered soils on airless bodies.

## 1. Introduction

Spectral observations of some parts of the lunar surface have long been shown to display unusual properties at visible and near-infrared (VNIR) wavelengths. The spectral shapes appear similar to those observed on Earth for minerals and rocks, but the darkest areas on the lunar surface are characterized by spectra with reduced band depths and steep red slopes (e.g., Adams & Jones, 1970; Fischer & Pieters, 1994; Hapke et al., 1970; Hawke et al., 2004). Today, we identify these optical effects as classic signs of space weathering of the lunar regolith.

Space weathering is the overarching term for the sum of processes affecting the lunar regolith, most broadly, the physical breakdown and vaporization from micrometeoroid bombardment, and chemical alteration from solar wind irradiation (e.g., Chapman, 2004; Noble et al., 2001; Pieters et al., 2000). Micrometeoroid bombardment physically breaks the regolith apart, vaporizes portions of it, and gardens the upper meters of the regolith (Hapke, 2001; Keller & McKay, 1993, 1997; Noble et al., 2001; Pieters & Noble 2016; Taylor et al., 2001). Solar wind affects the regolith by disrupting and damaging minerals and contributing to melting and volatilization (Hapke, 2001; Keller & McKay, 1997; Pieters et al., 2000). The vaporization and condensation of material causes the formation of amorphous and iron-rich agglutinates and mineral grain rims seen in Apollo samples, which

© 2023. The Authors.

This is an open access article under the terms of the [Creative Commons Attribution-NonCommercial-NoDerivs License](https://creativecommons.org/licenses/by/4.0/), which permits use and distribution in any medium, provided the original work is properly cited, the use is non-commercial and no modifications or adaptations are made.

manifest as optical effects in remote sensing data. Although the specific contributions from micrometeoroid bombardment and solar wind depend on the position in the solar system, the nature of space weathering means that it is a fundamental process of regolith maturation on any airless body (Noguchi et al., 2011, 2014; Pieters & Noble, 2016; Pieters et al., 2012). Therefore, the characterization of its effects on spectroscopic measurements is vital to correctly and quantitatively interpret remote sensing data.

In this study, we explore one optical effect of space weathering, darkening, on the midinfrared (MIR) region by measuring the spectra of silicates under lunar-like conditions. Because the lunar environment is thermally extreme, it is likely that the optical darkening caused by space weathering will affect the thermal gradient within lunar regolith, thus altering the spectra from what we would expect from spectral libraries acquired under ambient conditions. We test this idea by darkening three silicate particulate samples with nanophase carbon and analyzing the changes in their spectral features when measured under simulated lunar environment (SLE) conditions.

### 1.1. Known Effects of Space Weathering on IR Spectroscopy

Space weathering alters the optical properties of the lunar regolith in the VNIR range, as has been shown in early telescopic observations, as well as in the Clementine, Moon Mineralogy Mapper, and Kaguya data sets (e.g., Conel & Nash, 1970; Fischer & Pieters, 1996; Ohtake et al., 2010; Pieters et al., 2009) and in laboratory spectroscopic measurements of mature lunar soils (e.g., Adams & McCord, 1971a, 1971b; Pieters et al., 1993; Taylor et al., 2001). Spectra exhibit lower reflectance, reduction in band depth, and an overall red slope (decreasing reflectance with decreasing wavelength), all of which can make it more difficult to extract compositional information from the data. These effects appear to be a function of the degree of space weathering, as shown in remote sensing data (Fischer & Pieters, 1994, 1996; Keller et al., 1999; Pieters et al., 2000) and laboratory studies (Noble et al., 2007; Pieters et al., 2000; Sasaki et al., 2001; Yang et al., 2017).

Initial analyses of samples returned by the Apollo astronauts suggested that agglutinates might be the cause for the observed optical effects (e.g., Adams & McCord, 1970, 1971b; Conel & Nash, 1970), but advances in microscopic imaging techniques revealed the presence of amorphous nano-phase iron (npFe) rich rims on many mineral grains (e.g., Burgess & Stroud, 2018; Cassidy & Hapke, 1975; Keller & McKay, 1993, 1997; Pieters et al., 2000; Taylor et al., 1996, 2001; Thompson et al., 2016; Wentworth et al., 1999). These npFe rims are responsible for the optical changes observed in the VNIR: the darkening and shallowing of features due to their presence, and the red slope due to the size of the npFe, typically <30 nm (Burgess & Stroud, 2018; Housley et al., 1973; James et al., 2001; Keller & Clemett, 2001). The size of the particles is important as agglutinates also contain larger iron particles (Britt-Pieters particles; >~50 nm) that have been shown to lower the albedo without creating the red slopes in VNIR reflectance data (Britt & Pieters, 1994; Lucey & Noble, 2008; Lucey & Riner, 2011).

It was previously considered unlikely that space weathering would affect MIR spectra due to the penetration depth of MIR light (10's–100's of  $\mu\text{m}$ ) and the surficial nature (100's of nm) of space weathering coatings; MIR spectra are typically representative of bulk mineralogy and less influenced by minor or trace minerals in the sampled material than VNIR spectra (e.g., Salisbury et al., 1997). The overall optical effects due to space weathering in the VNIR were attributed to the npFe-rich amorphous rims in the regolith, an extremely minor component in the overall sample. Thus, it was thought that these rims would be too minor a volumetric component to contribute to the MIR spectrum. Additionally, a study by Moroz et al. (2014) determined that the amount of npFe generated through irradiation experiments would be insufficient to cause detectable optical darkening and attributed the albedo change to textural changes from micrometeorite bombardment. Several studies of meteoritic or impacted materials have indicated that the shock component of space weathering may also contribute to darkening of regolith and show shifts in MIR spectral features correlated with exposure to irradiation/shock (Morlok et al., 2017; Reitze et al., 2021; Weber et al., 2021).

Recent remote sensing studies (Glotch et al., 2015; Greenhagen et al., 2010; Kumari et al., 2020; Lucey et al., 2010, 2017) have characterized variation within the Diviner Lunar Radiometer Experiment (Diviner) data set that corresponds to recognized optical maturity (a measure for lunar space weathering) anomalies, including young crater rays and swirls, which also correspond to areas of albedo variation. Additionally, Brunetto et al. (2020) noted variations in the mid-to far-IR spectra from normal and irradiated meteorite spectra that suggest space weathering identifiers in remote data sets of OSIRIS-REx and James Webb Space Telescope.

The MIR includes numerous spectral features that are indicative of mineralogy, such as the Christiansen feature (CF), Reststrahlen bands (RBs), and transparency features (TFs). The CF is an emissivity maximum that shifts

position with the polymerization of the material, that is, highly polymerized silicates like quartz (and other felsic minerals) have shorter wavelength CF positions, whereas less polymerized minerals like olivine (and other mafic minerals) have long wavelength CF positions (Conel, 1969; Logan et al., 1973). Since 2009, Diviner has been collecting MIR thermal emission data, specifically targeted at defining the CF position, to constrain the bulk silicate composition of the Moon (Greenhagen et al., 2010; Paige et al., 2009).

The RBs are the fundamental vibrational bands that appear as emissivity minima caused by stretching and bending of Si-Al-O bonds. The spectral shapes, intensities and positions of the RBs are directly dependent on the mass of the atoms, strength of the bonds, lattice geometry, and physical properties (notably particle size), which directly correspond to the unique chemistry and structure of a mineral and can therefore be used as compositional identifiers (e.g., Conel, 1969; Cooper et al., 2002; Lyon, 1964). The TFs are emissivity minima with positions dependent on composition, and intensity dependent on particle size of the material, where fine particulates ( $< \sim 60 \mu\text{m}$ ) have lower emissivity at TFs due to increased scattering (e.g., Cooper et al., 2002).

Some laboratory studies have already shown correlations between MIR spectral feature shifts and space weathering in Apollo samples (Morlok et al., 2022) and irradiation experiments (Weber et al., 2021), while here, we focus on the darkening effect. By analyzing the effects of space weathering on these MIR features, combined with our previous knowledge of space weathering effects on VNIR spectra, we can use these data sets in tandem to create a more complete picture of lunar surface mineralogy.

## 1.2. Lunar Surface Conditions

The lunar surface environment differs substantially from Earth's, and previous laboratory studies have shown the importance of environmental conditions when measuring MIR spectra (Breitenfeld et al., 2021; Conel, 1969; Donaldson Hanna, Thomas, et al., 2012; Donaldson Hanna, Wyatt, et al., 2012; Donaldson Hanna et al., 2014, 2017; Henderson & Jakosky, 1997; Logan & Hunt, 1970; Nash et al., 1993; Salisbury et al., 1995; Shirley & Glotch, 2019). The lunar regolith is highly insulating, and a lack of atmosphere results in only limited heat transfer at grain-grain boundaries, a highly inefficient process. These properties, coupled with the exposure to the cold vacuum of space and heating from solar irradiation, set up a thermal gradient within the upper hundreds of microns of regolith. The thermal gradient was calculated by Henderson and Jakosky (1994, 1997) to be as high as 40 K/100  $\mu\text{m}$ . As a result of this thermal gradient, MIR spectra measured under SLE conditions display shifts in the positions of features and differences in contrast as compared to spectra measured under terrestrial ambient conditions.

Donaldson Hanna et al. (2017) have shown how variations in environmental conditions and soil maturity affect the CF position and the RB and TF strengths (i.e., spectral contrast) in MIR spectra. Based on the small changes observed in their study, along with work by Lucey et al. (2010, 2017) that noted a correlation between albedo and Diviner CF variation, we hypothesize that changes in the albedo of samples due to space weathering will alter the thermal properties of the regolith, resulting in changes in the MIR emissivity spectra.

## 2. Methods

### 2.1. Sample Description and Preparation

Samples in this study include anorthite, augite, and forsterite, chosen to represent a range of silicate polymerizations and silicates common on the Moon and other airless bodies. All samples are natural, ground to sand-sized particles ( $\sim 250 \mu\text{m}$ ) using an agate mortar and pestle, hand-picked, and assessed for quality using an optical microscope, traditional powder X-ray diffraction, and electron-probe microanalysis (see Shirley & Glotch, 2019 for further details). The samples were then further hand-ground and sieved to  $< 32 \mu\text{m}$  using an ATM Sonic Sifter. We added nano-phase carbon (npC; Alfa Aesar carbon black, acetylene, 50% compressed) to create a series of samples with varying albedo, defined as the reflectance at 750 nm determined using an ASD FieldSpec3 Max spectrometer at the Center for Planetary Exploration (CPEX) at Stony Brook University. Due to the small amount of sample, npC quantities are not reported, as amounts were below the  $10^{-4}$  g resolution of our balance.

### 2.2. Transmission Electron Microscopy of Nanophase Carbon

Because VNIR slopes and band depth changes have been shown to vary as a function of nanophase absorber particle size (Britt & Pieters, 1994; Legett, 2019; Lucey & Riner, 2011), we characterized the nanophase carbon

used in this study via transmission electron microscopy (TEM). Characterization of the lamp black carbon nanoparticles was performed at the Center for Functional Nanomaterials at Brookhaven National Laboratories. Phase analysis and purity were confirmed using a Rigaku Ultima III diffractometer equipped with a Cu anode with a wavelength of 1.54 Å.

An initial view of the particle size distributions and surface morphologies was achieved using a JEOL 7600F scanning electron microscope with further imaging being performed by TEM. TEM samples were created through sonication of an alcohol-carbon nanoparticle solution and then dropped onto a lacey carbon grid. The lacey carbon grid was placed in a Gatan single tilt holder and imaged under bright field conditions in a JEOL JEM 1400 TEM. Particle size distributions were calculated from the bright field images using Adobe Photoshop and measuring each particle in four directions and determining their average size of ~94 nm (Figure S1 in Supporting Information S1).

### 2.3. VNIR Reflectance Spectroscopy

All VNIR bidirectional reflectance spectra were acquired over the range of 0.35–2.5 μm at 1 nm spectral sampling under ambient conditions, measured at 0° emission angle and 30° incidence angle using an Analytical Spectral Devices Field Spec 3 Max Spectroradiometer located at CPEX. Spectra were acquired in a dark room behind a closed shroud to minimize the effects of stray light. Gain and offset detectors were optimized using a calibrated Spectralon standard before each sample was measured. A total of 100 scans each were collected of the sample, dark current, and the white reference, and three spectra were acquired for each sample and averaged.

### 2.4. SLE MIR Emissivity

After acquiring VNIR spectra, samples were poured into 2.3 cm diameter aluminum sample cups to maintain a rough surface similar to what would be expected for a natural regolith surface, and then loaded into the Planetary and Asteroid Regolith Spectroscopy Environmental Chamber (PARSEC) at CPEX for MIR emissivity measurements. PARSEC is designed to measure up to six samples per run under environmental conditions of airless planetary bodies. Samples were measured under ambient conditions, followed by measurement under SLE conditions. Ambient conditions are defined as pressure at 1,000 mbar, chamber temperature at ~300 K, sample temperature at 350 K, with no external illumination. SLE conditions are achieved by pumping the chamber down to a pressure of  $<10^{-5}$  mbar, heating the samples from below to 350 K, heating from above via 75 W quartz halogen lamp connected to a tunable power source, and cooling the chamber to  $<150$  K. The PARSEC cold shield is actively cooled via input of liquid nitrogen into an internal dewar, and pressure is controlled by a Pfeiffer HiCube turbo vacuum pump. PARSEC is connected to a Nicolet 6700 FTIR spectrometer equipped with a KBr beamsplitter and a deuterated L-alanine doped triglycine sulfate (DLATGS) detector with a KBr window, measuring the thermal emission across 400–2,200  $\text{cm}^{-1}$  with a spectral sampling of 2  $\text{cm}^{-1}$ . The spectrometer was actively purged with air scrubbed of  $\text{CO}_2$  and water vapor. Measurements of a black body target in PARSEC are acquired at 340 and 370 K at the beginning of each series of measurements for use in the calibration. Due to a ~1 cm gap between the spectrometer and chamber, some spectra show features due to atmospheric water, notably in the region shortward of 1,200  $\text{cm}^{-1}$ .

Emission spectra acquired under ambient conditions were calibrated according to the methods of Ruff et al. (1997), while spectra acquired under SLE conditions were calibrated using the methods of Thomas et al. (2012). A polynomial was fitted to the ~1,100–1,300  $\text{cm}^{-1}$  portion of each spectrum (range dependent on mineral for best fitting), and the frequency of the maximum of the fit was used to define the CF position in the manner of Donaldson Hanna, Wyatt, et al. (2012). To examine the spectral contrast, the first RB minimum longward of the CF was used to determine changes in band depth with albedo. Comparisons of the band depth of the TFs were made by fitting a continuum to the peaks on either side of the TF region (~600–900  $\text{cm}^{-1}$  dependent on the mineral), finding the frequency of the TF minimum of the set of ambient or SLE spectra, and calculating the difference in emissivity at this wavelength between the continuum and spectrum for each sample per mineral. To examine the spectral contrast of the TF region at shorter frequency/longer wavenumbers than the CF (~1,150–1,450  $\text{cm}^{-1}$ , exact range dependent on mineral), the slope was measured between two points ~100  $\text{cm}^{-1}$  apart.

## 3. Results

### 3.1. VNIR Spectra

The samples show general trends of decreasing albedo and loss of spectral features with the addition of increasing amounts of npC. Figure 1 shows the VNIR spectra for anorthite, which show that with decreasing albedo, the

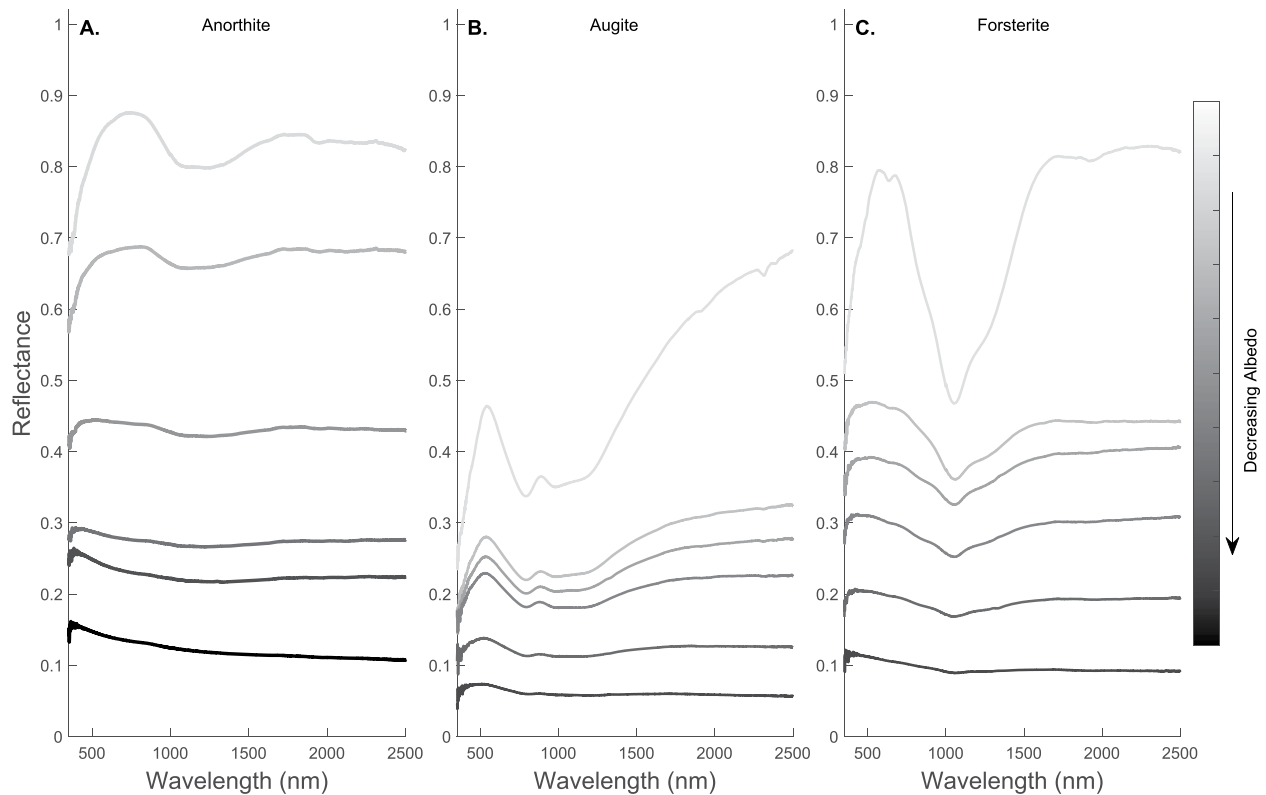


**Figure 1.** VNIR reflectance spectra of  $<32\ \mu\text{m}</math> anorthite (a), augite (b), and forsterite (c) darkened from pure (gray) with increasing amounts of npC to the lowest albedo (black). Overall reflectance decreases, and spectral features are lost with increasing npC addition; however, no reddening is observed likely due to the large npC particle size.$

broad feature around 1,200 nm becomes less prominent. The same can be seen for augite (feature around 800 nm) and for forsterite (feature around 1,000 nm).

### 3.2. MIR Spectra

The SLE MIR emissivity spectra for anorthite show variation within the spectra on a larger scale than observed in the ambient data (Figures 2a, 2d, and 2g). The ambient CF position is  $1,240 \pm 4\ \text{cm}^{-1}$  but under SLE shifts to longer wavelengths with increasing npC content by  $\sim 40\ \text{cm}^{-1}$  or  $\sim 0.28\ \mu\text{m}$  (Figure 3a). The RBs decrease in spectral contrast with increasing npC content, with emissivity increasing by 0.25 between the pure and most darkened samples under SLE conditions compared to a shift of only 0.02 under ambient conditions. The broad TF region shortward of the CF position increases in emissivity with increasing npC content, as does the TF at  $818\ \text{cm}^{-1}$ , though when compared against a continuum, the band depth only changes by 0.01 for SLE and 0.02 for ambient spectra.

Augite SLE MIR emissivity spectra show more variation within the spectra than observed in the ambient data (Figures 2b, 2e, and 2h). The CF position shifts by  $\sim 20\ \text{cm}^{-1}$  or  $0.14\ \mu\text{m}$ . The RB decreases in spectral contrast with increasing npC content, with emissivity increasing by 0.07 between the pure and most darkened samples, as compared to a shift of only 0.02 under ambient conditions. The TF shortward of the CF position increases in emissivity with increasing npC content with similar slope changes under both ambient and SLE conditions, though the TF at  $740\ \text{cm}^{-1}$  compared the continuum changes by only 0.03 under ambient conditions and 0.02 under SLE.

The SLE MIR emissivity spectra of forsterite show greater variation within the spectra than observed in the ambient data (Figures 2c, 2f, and 2i). The CF position shifts to longer wavelengths with increasing npC content by  $\sim 35\ \text{cm}^{-1}$  or  $0.24\ \mu\text{m}$ . The RB decreased in spectral contrast with increasing npC content, with emissivity increasing by 0.15 between the pure and most darkened samples compared to 0.05 under ambient conditions.

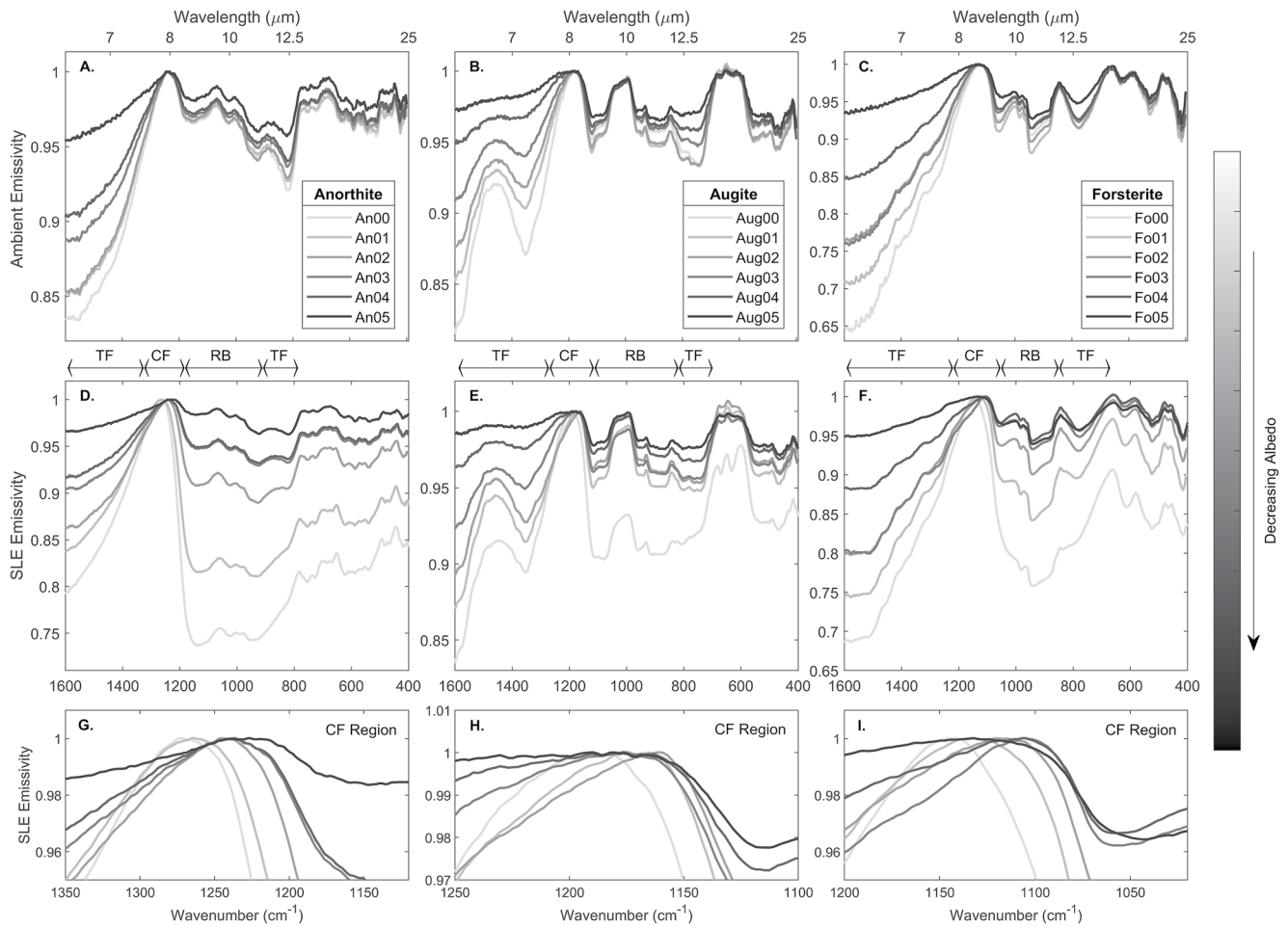


**Figure 2.** MIR emissivity spectra of anorthite (a, d, g), augite (b, e, h), and forsterite (c, f, i) under both ambient (top row) and simulated lunar environment (SLE) conditions (middle row). Samples are colored gray to black showing increasing npC content. All show shallowing of spectra with increasing npC content, though by a much greater margin in SLE conditions. SLE spectra show a shift in the Christiansen Feature position to longer wavelengths with increasing npC (bottom row). Regions of investigated features are labeled.

The TF shortward of the CF position increases in emissivity with increasing npC content, and the band depth of the TF at  $773\text{ cm}^{-1}$  decreases with decreasing reflectance by 0.03 under ambient conditions and changes by 0.02 for SLE.

## 4. Discussion

### 4.1. Spectral Trends

The VNIR spectra for the npC darkened samples show similar characteristics to naturally and experimentally space-weathered material, including decreases in reflectance and band depth. The absence of red slopes in the spectra is likely due to the size of npC used in our experiment. TEM measurements of the npC used in this study found an average diameter of 94 nm (Figure S1 in Supporting Information S1), much larger than the npFe found in lunar regolith rims ( $<10\text{ nm}$ ). However, the npC particle size is within the size range of Britt-Pieters particles found in lunar agglutinates, which cause darkening but not reddening (Britt & Pieters, 1994; Lucey & Noble, 2008; Lucey & Riner, 2011).

The most notable changes in the SLE MIR data are the decrease in overall spectral contrast and the shift in CF position to longer wavelengths with decreasing albedo of the samples. The shift in CF position appears to be linear for anorthite, roughly linear for forsterite, and no obvious trend for augite (Figure 3a). There is a small offset among the trends that is consistent with the range of albedo of the pure minerals, that is, anorthite is the

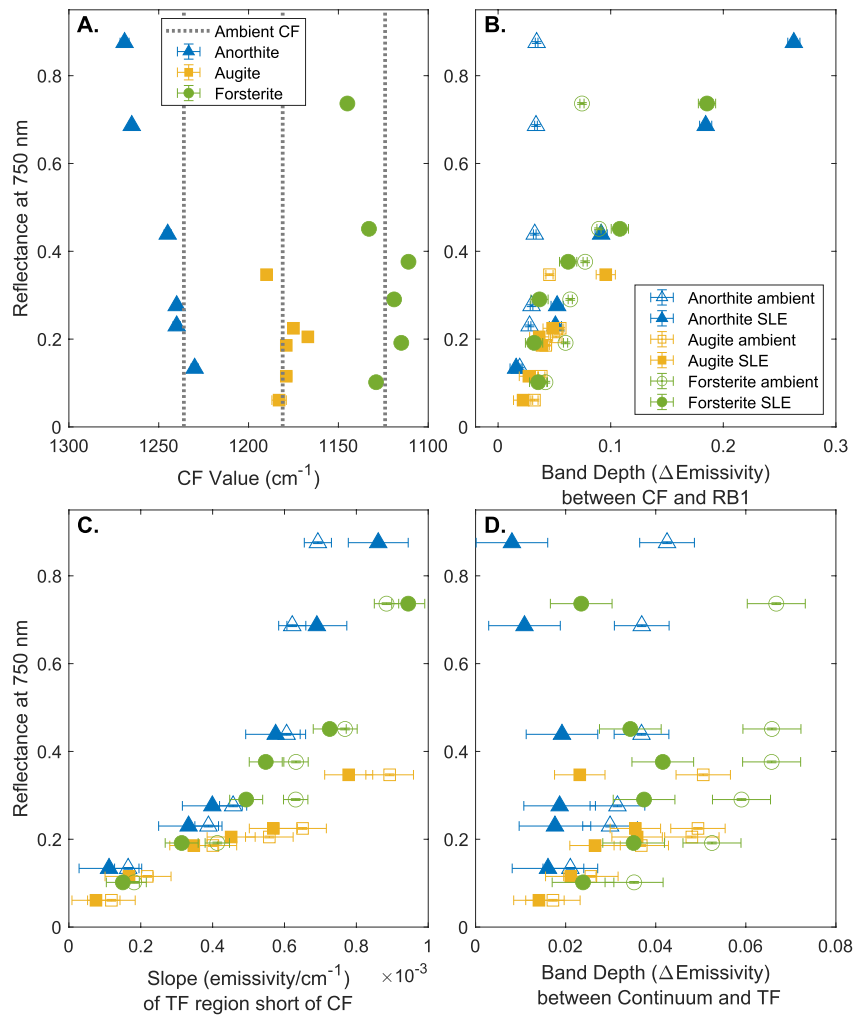


**Figure 3.** Variation of the Christiansen Feature (CF) value position (a), first Reststrahlen band depth (b), slope of the transparency feature (TF) region at shorter wavelengths/longer wavenumbers than the CF (c), and band depth from a continuum at the TF (d) compared to albedo per mineral.

brightest pure mineral sample, so has the largest range of albedo and steepest slope in the CF-albedo trend, whereas augite, with the smallest range of albedo change, has almost no CF variation. This trend points to a link between the inherent albedo of a mineral and the range of thermal gradients it will experience. That is, minerals with lower inherent albedos (naturally darker minerals) absorb more solar radiation, and therefore experience a less pronounced thermal gradient, leading to less MIR spectral variation than their higher albedo counterparts.

The change in spectral contrast was examined by looking at the band depth of the first RB at wavelengths longward of the CF (occurring at  $\sim 1,200\text{--}1,050\text{ cm}^{-1}$ , Figure 3b). The trend in RB spectral contrast is similar to the trend in CF variation in that the anorthite and forsterite have much more pronounced differences in band depth between the ambient and SLE spectra, again likely due to their inherent brighter albedo. Increasing emissivity in the RBs with decreasing the albedo of the sample is likely due to changes in the thermal gradient caused by the darkening. The RB region of the spectrum just longward of the CF position samples material from shallower depths than other spectral regions due to the higher absorption coefficient values at the RB, which, for bright material, means that the RBs sample cooler material. However, with the decrease in albedo, the thermal gradient is reduced, resulting in a reduced spectral contrast in the spectra.

There are two main TF regions that we see affected by the darkening with npC: the region ( $\sim 1,600\text{--}1,200\text{ cm}^{-1}$ ) short of the CF and the TF near  $\sim 750\text{--}850\text{ cm}^{-1}$ . The TF region short of the CF exhibits a strong trend of decreasing slope with decreasing albedo with little difference in values between ambient and SLE spectra (Figure 3c).

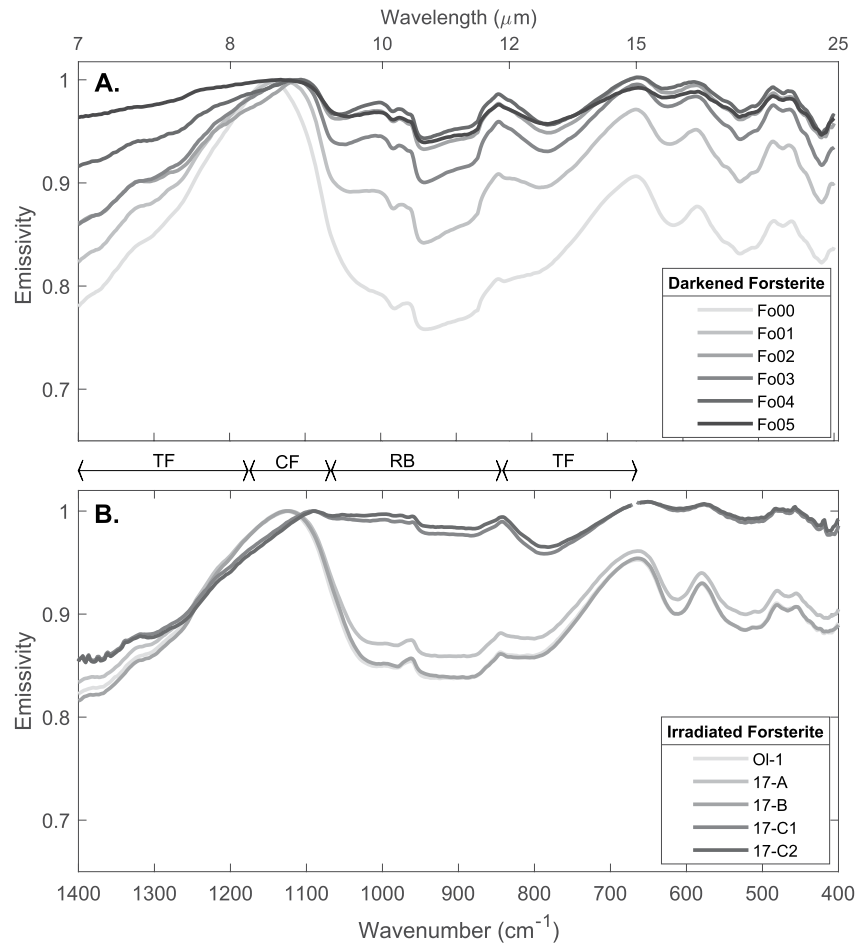


**Figure 4.**  $<32 \mu\text{m}$  carbon-darkened forsterite (a) and laser-irradiated forsterite (b) MIR emissivity spectra measured under simulated lunar environment conditions with a gray-scale to indicate pure forsterite to most “weathered.” Both sets of spectra show a loss of spectral contrast, and a shift in the Christiansen Feature position to a longer wavelength with increasing npC/irradiation. Regions of investigated features are labeled.

There is some variation with albedo in the longer wavelength region near  $800 \text{ cm}^{-1}$ ,  $<0.03$  for each mineral under the same set of conditions and  $\sim 0.04$  difference between ambient and SLE conditions for the brightest samples. The ambient trends for both TF regions are similar, but the SLE spectra show a change in the first TF region that is much less prominent at the second. We hypothesize that this is due to the ways in which these different wavelength regions are affected by temperature under the SLE conditions: the shortwave TF region is sensing a deeper and therefore warmer layer of sample that the highly absorbing npC is helping to warm, thus producing the change in slope with albedo, but the longwave TF region is sensing a shallower and thus cooler depth, producing a more consistent feature representative of the scattering from the overall small particle size of the sample with limited change due to the added npC (Figure 3d).

#### 4.2. Comparison to Irradiated Samples

The shifts observed in the CF for darkened samples are similar to the overall shift seen in experimentally space-weathered olivine samples from Yang et al. (2017) (Figure 4). Yang et al. (2017) conducted pulse laser irradiation experiments of varying intensity resulting in a series of olivine powders with varying degrees of space weathering that exhibit typical VNIR spectral changes and also show variation in the MIR under SLE conditions. For comparison, Figure 5a shows CF shifts with albedo for forsterite samples from Yang et al. (2017) as compared to our darkened forsterite. Because of the importance of particle size (Shirley & Glotch, 2019), we included another size fraction of forsterite ( $<63 \mu\text{m}$ ) darkened with npC to compare with Yang et al. (2017)  $<45 \mu\text{m}$  forsterite samples. The three sample sets show similar trends in CF shift with albedo, with two offsets:

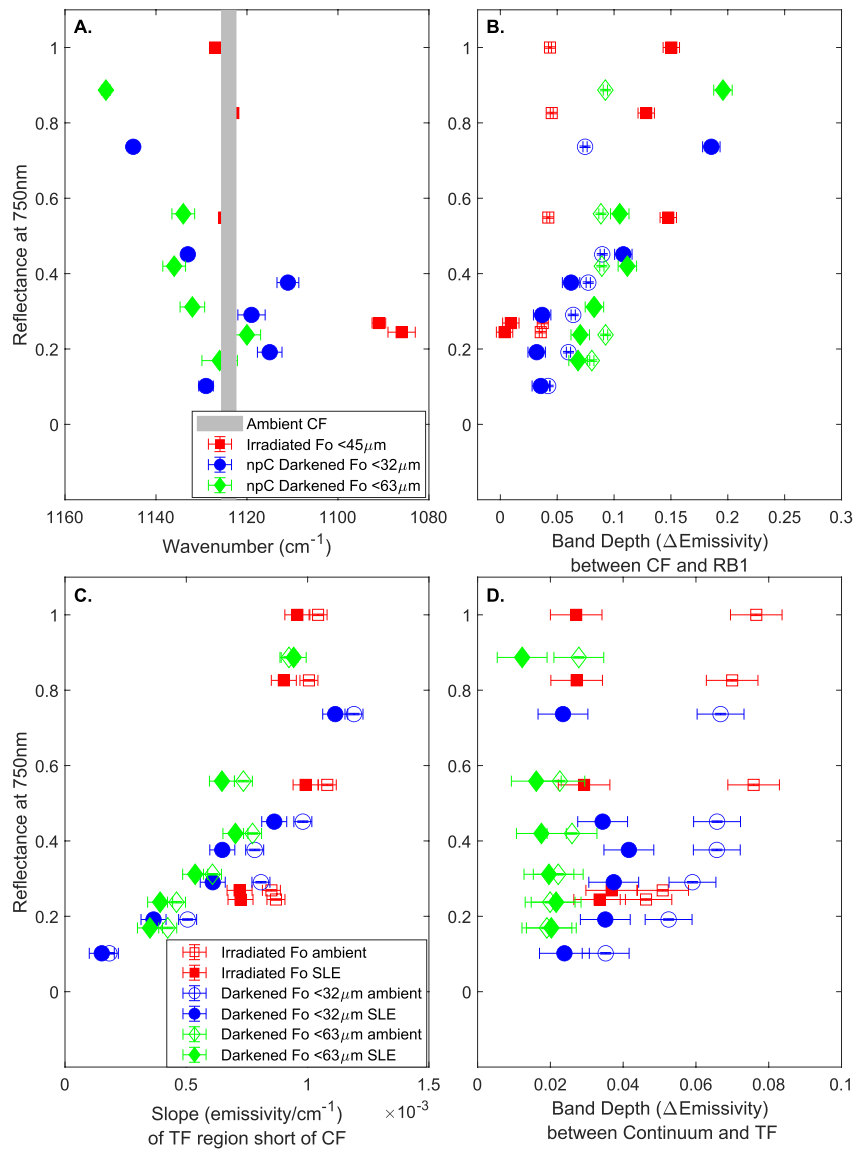


**Figure 5.** Variation of the Christiansen Feature (CF) value (a), the band depth of the first Reststrahlen band (b), the slope of the transparency feature (TF) region at shorter wavelength/longer wavenumber to the CF (c), and the band depth from a continuum of the TF (d) as compared to the albedo of the sample. The irradiated samples from Yang et al. (2017) are in red, and two size fractions of npC-darkened forsterite (<32  $\mu\text{m}$  in blue, and <63  $\mu\text{m}$  in green) are shown for comparison.

(a) the small shift between the two npC samples due to particle size, which is in line with previous observations of smaller particle size having shorter wavelength (longer wavenumber) CF positions under SLE (Shirley & Glotch, 2019); and (b) the longer wavelength (shorter wavenumber) CF positions for the irradiated samples due to the forsterite used by Yang et al. (2017, 2021) being of slightly different Fo#.

The MIR spectral contrast also varies between the irradiated and darkened samples. The variation in the first RB ( $\sim 1,050 \text{ cm}^{-1}$ ; Figure 5b) under ambient conditions is  $< 0.05$  for all forsterite sets, but under SLE this increases to 0.15 with increasing albedo. The gradual change in the darkened forsterite versus the more abrupt change in the Yang et al. (2017) samples may be due to the size of the absorber and how it is incorporated into the sample. The synthetic space weathering forms npFe within the grains that darkens the samples more quickly with a different size and abundance of absorbers than that of the npC, which is simply mixed into the sample, not altering the grains. In other words, the difference may be due to many small inclusions of npFe versus many large, separate npC particles.

The variations in spectral contrast in the first TF region ( $\sim 1,400\text{--}1,200 \text{ cm}^{-1}$ , Figure 5c) are likely also due to the size of the npC used in this experiment as we do not see a similar change in the Yang et al. (2017) MIR spectra.

We hypothesize that this TF region is sensing deeper into the sample than the RBs and therefore, a warmer part of the thermal gradient than the npC, possibly due to its size or thermal properties, is affecting more than the npFe. At the  $780\text{ cm}^{-1}$  TF (Figure 5d), the  $<63\text{ }\mu\text{m}$  size fraction shows  $<0.01$  change in band depth under both ambient and SLE conditions due to the larger size fraction, while the  $<32\text{ }\mu\text{m}$  and  $<45\text{ }\mu\text{m}$  exhibit similar variations in band depth:  $\sim 0.03$  change with albedo under ambient and  $\sim 0.01$  under SLE. As discussed above, there are stark differences in the behavior of these TF regions dependent on measurement conditions, but here we also see the effect of particle size: there is little variation in the longwave TF region band depth for the  $<63\text{ }\mu\text{m}$  sample under both conditions, unlike the  $<45\text{ }\mu\text{m}$  and  $<32\text{ }\mu\text{m}$  samples. Additionally, the overall decrease in band depth under SLE may indicate that the longwave TF is less detectable on airless bodies, so may not be as useful for mineral identification or grain size information as the slope of the shortwave TF region.

Recent studies comparing MIR spectral features to maturity of Apollo samples (Morlok et al., 2022) have shown trends of decreasing spectral contrast between the CF and RB/TFs with increasing soil maturity. This spectral contrast variation is similar to the TF band depth variation observed in our data when measured under ambient conditions; however, as their data were not measured under SLE, it is unclear whether we would see similar shifts in behavior due to temperature. While this is not an exact comparison to the features discussed here, it does provide support for the investigation of space weathering in interpreting lunar data.

### 4.3. Comparison to Diviner Data

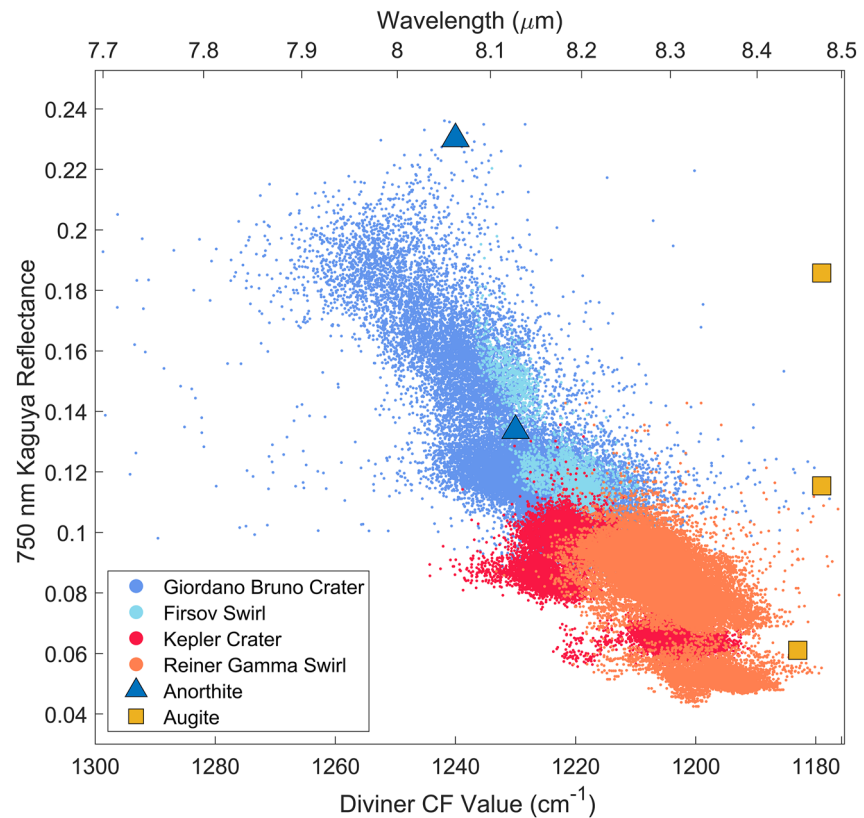
When compared to variations observed in the remote sensing data sets, we see there are some similarities in the shift of CF values with albedo; however, it is difficult to do a direct comparison between minerals measured under laboratory conditions and lunar regolith. The remote data sets show linear trends between Diviner CF value against Kaguya 750 nm reflectance, but not at the extreme slopes seen in the laboratory data. To investigate regions with variable space weathering, but likely little compositional differences, we investigated several locations discussed by Lucey et al. (2017) that show evidence for optical maturity variation. These regions of interest are fresh craters and lunar swirls that occur in both highlands and mare terrains (Kepler Crater, Reiner Gamma Swirl, Giordano Bruno Crater, and Firsov Swirl). We used Optical Maturity index data in conjunction with Wide-Angle Camera mosaics of the regions to examine areas with variable maturity and to pick out areas within the crater ejecta, or on- and off-swirls as well as background regions that appeared relatively unaffected by the feature.

Figure 6 shows 750 nm albedo versus CF value for these four locations with the overlapping laboratory data-points for comparison. As we saw in the laboratory data, there is a larger range of albedo shown in the highlands locations (Giordano Bruno and Firsov) by virtue of the material being inherently brighter. There is an interesting variability between these sites and the trends observed at each site, notably that the swirls exhibit steeper trends than the craters, likely due to the difference in how space weathering affects the magnetic anomalies versus truly fresh material, or the fact that the swirls are smaller areas, so may exhibit less compositional variability than the larger craters. The shallower trends in the lunar data also reflect a larger change in CF over similar changes in reflectance when compared to the laboratory data. This difference in CF value is likely due to either more variability in the lunar soils over the large (km-scale) regions studied, or simply the higher variability in CF captured by rocks versus pure minerals. For a more in-depth analysis of the relationship between soil maturity, albedo, and CF value at fresh craters and swirls, see Kumari et al. (2020).

## 5. Conclusions

In this work, we observe variations in MIR spectra under SLE conditions caused by albedo, which we use as a proxy for space weathering. These variations include shifts in the CF position, generally to longer wavelengths, and a decrease in spectral contrast with decreasing albedo. Our results are comparable to changes seen in both synthetic space weathering via laser pulse irradiation experiments (Yang et al., 2017), and those seen in Apollo samples of varying maturity (Donaldson Hanna et al., 2015). These variations, therefore, seem to mainly be caused by the changes in albedo from the cumulative effects of space weathering, and not solely from the creation of amorphous rims and npFe that produce optical effects in the VNIR but are volumetrically insignificant at the penetration depths of MIR measurements.

Additionally, the shift in the CF position to longer wavelengths with decreasing albedo produces CF values that occur at longer wavelengths than measured under the typical ambient conditions of most spectral libraries. Therefore, we must take albedo into account when analyzing remote sensing data from airless bodies and can use



**Figure 6.** Comparison of Christiansen Feature value to albedo between fresh craters (dark blue and red) and lunar swirls (light blue and orange), highlands (blues) and mare (reds) material, and overlapping laboratory data points (triangles and squares from Figure 3a).

this and future work, including data from upcoming remote and sample-return missions, to develop a calibration method that combines remote observations with laboratory analysis for improved compositional interpretation.

## Data Availability Statement

Data used in this manuscript are available at <http://doi.org/10.5281/zenodo.7236130> (Shirley et al., 2023).

## Acknowledgments

This work was supported by the Lunar Reconnaissance Orbiter 5th Extended Science Mission and the RISE2 node of NASA's Solar System Exploration Research Virtual Institute (Cooperative Agreement Number 80NSSC19M0215).

## References

- Adams, J. B., & Jones, R. L. (1970). Spectral reflectivity of lunar samples. *Science*, *167*(3918), 737–739. <https://doi.org/10.1126/science.167.3918.737>
- Adams, J. B., & McCord, T. B. (1970). Remote sensing of lunar surface mineralogy: Implications from visible and near-infrared reflectivity of Apollo 11 samples. *Geochimica et Cosmochimica Acta - Supplement*, *1*.
- Adams, J. B., & McCord, T. B. (1971a). Alteration of lunar optical properties: Age and composition effects. *Science*, *171*(3971), 567–571. <https://doi.org/10.1126/science.171.3971.567>
- Adams, J. B., & McCord, T. B. (1971b). Optical properties of mineral separates, glass, and anorthositic fragments from Apollo mare samples. In *Lunar and planetary science conference proceedings* (Vol. 2, p. 2183).
- Breitenfeld, L. B., Rogers, A. D., Glotch, T. D., Hamilton, V. E., Christensen, P. R., Lauretta, D. S., et al. (2021). Machine learning mid-infrared spectral models for predicting modal mineralogy of CI/CM chondritic asteroids and Bennu. *Journal of Geophysical Research: Planets*, *126*(12), e2021JE007035. <https://doi.org/10.1029/2021je007035>
- Britt, D. T., & Pieters, C. M. (1994). Darkening in black and gas-rich ordinary chondrites: The spectral effects of opaque morphology and distribution. *Geochimica et Cosmochimica Acta*, *58*(18), 3905–3919. [https://doi.org/10.1016/0016-7037\(94\)90370-0](https://doi.org/10.1016/0016-7037(94)90370-0)
- Brunetto, R., Lantz, C., Nakamura, T., Baklouti, D., Le Pivert-Jolivet, T., Kobayashi, S., & Borondics, F. (2020). Characterizing irradiated surfaces using IR spectroscopy. *Icarus*, *345*, 113722. <https://doi.org/10.1016/j.icarus.2020.113722>
- Burgess, K. D., & Stroud, R. M. (2018). Coordinated nanoscale compositional and oxidation state measurements of lunar space-weathered material. *Journal of Geophysical Research: Planets*, *123*(8), 2022–2037. <https://doi.org/10.1029/2018JE005537>
- Cassidy, W., & Hapke, B. (1975). Effects of darkening processes on surfaces of airless bodies. *Icarus*, *25*(3), 371–383. [https://doi.org/10.1016/0019-1035\(75\)90002-0](https://doi.org/10.1016/0019-1035(75)90002-0)
- Chapman, C. R. (2004). Space weathering of asteroid surfaces. *Annual Review of Earth and Planetary Sciences*, *32*(1), 539–567. <https://doi.org/10.1146/annurev.earth.32.101802.120453>

- Conel, J. E. (1969). Infrared emissivities of silicates: Experimental results and a cloudy atmospheric model of spectral emission from condensed particulate mediums. *Journal of Geophysical Research*, 74(6), 1614–1634. <https://doi.org/10.1029/JB074i006p01614>
- Conel, J. E., & Nash, D. B. (1970). Spectral reflectance and albedo of Apollo 11 lunar samples: Effects of irradiation and vitrification and comparison with telescopic observations. *Geochimica et Cosmochimica Acta - Supplement*, 1.
- Cooper, B. L., Salisbury, J. W., Killen, R. M., & Potter, A. E. (2002). Midinfrared spectral features of rocks and their powders. *Journal of Geophysical Research*, 107(E4), 5017. <https://doi.org/10.1029/2000je001462>
- Donaldson Hanna, K. L., Bowles, N. E., Pieters, C. M., Greenhagen, B. T., Glotch, T. D., & Lucey, P. G. (2015). Effects of space weathering on thermal infrared emissivity spectra of bulk lunar soils measured under simulated lunar conditions. In *Space weathering of airless bodies: An integration of remote sensing data* (Vol. 1878, p. 2020). Laboratory Experiments and Sample Analysis Workshop.
- Donaldson Hanna, K. L., Cheek, L. C., Pieters, C. M., Mustard, J. F., Greenhagen, B. T., Thomas, I. R., & Bowles, N. E. (2014). Global assessment of pure crystalline plagioclase across the Moon and implications for the evolution of the primary crust. *Journal of Geophysical Research: Planets*, 119(7), 1516–1545. <https://doi.org/10.1002/2013je004476>
- Donaldson Hanna, K. L., Greenhagen, B. T., Patterson, W. R., Pieters, C. M., Mustard, J. F., Bowles, N. E., et al. (2017). Effects of varying environmental conditions on emissivity spectra of bulk lunar soils: Application to Diviner thermal infrared observations of the Moon. *Icarus*, 283, 326–342. <https://doi.org/10.1016/j.icarus.2016.05.034>
- Donaldson Hanna, K. L., Thomas, I. R., Bowles, N. E., Greenhagen, B. T., Pieters, C. M., Mustard, J. F., et al. (2012). Laboratory emissivity measurements of the plagioclase solid solution series under varying environmental conditions. *Journal of Geophysical Research*, 117(E11), E11004. <https://doi.org/10.1029/2012JE004184>
- Donaldson Hanna, K. L., Wyatt, M. B., Thomas, I. R., Bowles, N. E., Greenhagen, B. T., Maturilli, A., et al. (2012). Thermal infrared emissivity measurements under a simulated lunar environment: Application to the Diviner Lunar Radiometer Experiment. *Journal of Geophysical Research*, 117(E12), E00H05. <https://doi.org/10.1029/2011JE003862>
- Fischer, E. M., & Pieters, C. M. (1994). Remote determination of exposure degree and iron concentration of lunar soils using VIS-NIR spectroscopic methods. *Icarus*, 111(2), 475–488. <https://doi.org/10.1006/icar.1994.1158>
- Fischer, E. M., & Pieters, C. M. (1996). Composition and exposure age of the Apollo 16 Cayley and Descartes regions from Clementine data: Normalizing the optical effects of space weathering. *Journal of Geophysical Research*, 101(E1), 2225–2234. <https://doi.org/10.1029/95je02983>
- Glotch, T. D., Bandfield, J. L., Lucey, P. G., Hayne, P. O., Greenhagen, B. T., Arnold, J. A., et al. (2015). Formation of lunar swirls by magnetic field standoff of the solar wind. *Nature Communications*, 6(1), 6189. <https://doi.org/10.1038/ncomms7189>
- Greenhagen, B. T., Lucey, P. G., Wyatt, M. B., Glotch, T. D., Allen, C. C., Arnold, J. A., et al. (2010). Global silicate mineralogy of the Moon from the diviner lunar radiometer. *Science*, 329(5998), 1507–1509. <https://doi.org/10.1126/science.1192196>
- Hapke, B. (2001). Space weathering from Mercury to the asteroid belt. *Journal of Geophysical Research*, 106(E5), 10039–10074. <https://doi.org/10.1029/2000je001338>
- Hapke, B. W., Cohen, A. J., Cassidy, W. A., & Wells, E. N. (1970). Solar radiation effects on the optical properties of Apollo 11 samples. *Geochimica et Cosmochimica Acta - Supplement*, 1, 2199.
- Hawke, B. R., Blewett, D. T., Lucey, P. G., Smith, G. A., Bell, J. F., III, Campbell, B. A., & Robinson, M. S. (2004). The origin of lunar crater rays. *Icarus*, 170(1), 1–16. [https://doi.org/10.1016/s0019-1035\(04\)00070-3](https://doi.org/10.1016/s0019-1035(04)00070-3)
- Henderson, B. G., & Jakosky, B. M. (1994). Near-surface thermal gradients and their effects on mid-infrared emission spectra of planetary surfaces. *Journal of Geophysical Research*, 99(E9), 19063–19073. <https://doi.org/10.1029/94je01861>
- Henderson, B. G., & Jakosky, B. M. (1997). Near-surface thermal gradients and mid-IR emission spectra: A new model including scattering and application to real data. *Journal of Geophysical Research*, 102(E3), 6567–6580. <https://doi.org/10.1029/96je03781>
- Housley, R. M., Grant, R. W., & Paton, N. E. (1973). Origin and characteristics of excess Fe metal in lunar glass welded aggregates. In *Proceedings lunar and planetary science conference* (Vol. 4, pp. 2737–2749).
- James, C. L., Basu, A., Wentworth, S. J., & McKay, D. S. (2001). Grain size distribution of Fe<sup>0</sup> globules in lunar agglutinitic glass: First results from Apollo 17 Soil 78.421. In *GSA annual meeting*.
- Keller, L. P., & Clemett, S. J. (2001). Formation of nanophase iron in the lunar regolith. *Lunar and Planetary Science*, XXXII. Abstract 2097.
- Keller, L. P., & McKay, D. S. (1993). Discovery of vapor deposits in the lunar regolith. *Science*, 261(5126), 1305–1307. <https://doi.org/10.1126/science.261.5126.1305>
- Keller, L. P., & McKay, D. S. (1997). The nature and origin of rims on lunar soil grains. *Geochimica et Cosmochimica Acta*, 61(11), 2331–2341. [https://doi.org/10.1016/s0016-7037\(97\)00085-9](https://doi.org/10.1016/s0016-7037(97)00085-9)
- Keller, L. P., Wentworth, S. J., McKay, D. S., Taylor, L. A., Pieters, C., & Morris, R. V. (1999). Space weathering in the fine size fractions of lunar soils: Soil maturity effects. In *New views of the Moon 2: Understanding the moon through the integration of diverse data sets* (p. 32).
- Kumari, N., Glotch, T. D., & Shirley, K. A. (2020). Investigation of variation in Christiansen feature with albedo on the Moon using the diviner, M3, and Kaguya data sets. LPSC. Abstract 1967.
- Legett, C. L. I. V. (2019). Novel theoretical and experimental approaches to understanding the spectral effects of space weathering generated nanoparticles. Ph.D. Thesis, Stony Brook University.
- Logan, L. M., & Hunt, G. R. (1970). Emission spectra of particulate silicates under simulated lunar conditions. *Journal of Geophysical Research*, 75(32), 6539–6548. <https://doi.org/10.1029/JB075i032p06539>
- Logan, L. M., Hunt, G. R., Salisbury, J. W., & Balsamo, S. R. (1973). Compositional implications of Christiansen frequency maximums for infrared remote sensing applications. *Journal of Geophysical Research*, 78(23), 4983–5003. <https://doi.org/10.1029/JB078i023p04983>
- Lucey, P. G., Greenhagen, B. T., Song, E., Arnold, J. A., Lemelin, M., Hanna, K. D., et al. (2017). Space weathering effects in diviner lunar radiometer multispectral infrared measurements of the lunar Christiansen Feature: Characteristics and mitigation. *Icarus*, 283, 343–351. <https://doi.org/10.1016/j.icarus.2016.05.010>
- Lucey, P. G., & Noble, S. K. (2008). Experimental test of a radiative transfer model of the optical effects of space weathering. *Icarus*, 197(1), 348–353. <https://doi.org/10.1016/j.icarus.2008.05.008>
- Lucey, P. G., Paige, D. A., Greenhagen, B. T., Bandfield, J. L., & Glotch, T. D. (2010). Comparison of diviner Christiansen feature position and visible albedo: Composition and space weathering implications. *Lunar and Planetary Science Conference*, 41, 1600.
- Lucey, P. G., & Riner, M. A. (2011). The optical effects of small iron particles that darken but do not redden: Evidence of intense space weathering on Mercury. *Icarus*, 212(2), 451–462. <https://doi.org/10.1016/j.icarus.2011.01.022>
- Lyon, R. J. P. (1964). Evaluation of infrared spectrophotometry for compositional analysis of lunar and planetary soils. Part II—rough and powdered surfaces (No. NASA-CR-100).
- Morlok, A., Bischoff, A., Patzek, M., Sohn, M., & Hiesinger, H. (2017). Chelyabinsk—a rock with many different (stony) faces: An infrared study. *Icarus*, 284, 431–442. <https://doi.org/10.1016/j.icarus.2016.11.030>

- Morlok, A., Joy, K. H., Martin, D., Wogelius, R., & Hiesinger, H. (2022). Laboratory IR spectroscopy of soils from Apollo 14, 15, and 16: Spectral parameters and maturity. *Planetary and Space Science*, 223, 105576. <https://doi.org/10.1016/j.pss.2022.105576>
- Moroz, L. V., Starukhina, L. V., Rout, S. S., Sasaki, S., Helbert, J., Baither, D., et al. (2014). Space weathering of silicate regoliths with various FeO contents: New insights from laser irradiation experiments and theoretical spectral simulations. *Icarus*, 235, 187–206. <https://doi.org/10.1016/j.icarus.2014.03.021>
- Nash, D. B., Salisbury, J. W., Conel, J. E., Lucey, P. G., & Christensen, P. R. (1993). Evaluation of infrared emission spectroscopy for mapping the Moon's surface composition from lunar orbit. *Journal of Geophysical Research*, 98(E12), 23535–23552. <https://doi.org/10.1029/93je02604>
- Noble, S. K., Pieters, C. M., & Keller, L. P. (2007). An experimental approach to understanding the optical effects of space weathering. *Icarus*, 192(2), 629–642. <https://doi.org/10.1016/j.icarus.2007.07.021>
- Noble, S. K., Pieters, C. M., Taylor, L. A., Morris, R. V., Allen, C. C., McKay, D. S., & Keller, L. P. (2001). The optical properties of the finest fraction of lunar soil: Implications for space weathering. *Meteoritics & Planetary Sciences*, 36(1), 31–42. <https://doi.org/10.1111/j.1945-5100.2001.tb01808.x>
- Noguchi, T., Kimura, M., Hashimoto, T., Konno, M., Nakamura, T., Zolensky, M. E., et al. (2014). Space weathered rims found on the surfaces of the Itokawa dust particles. *Meteoritics & Planetary Sciences*, 49(2), 188–214. <https://doi.org/10.1111/maps.12111>
- Noguchi, T., Nakamura, T., Kimura, M., Zolensky, M. E., Tanaka, M., Hashimoto, T., et al. (2011). Incipient space weathering observed on the surface of Itokawa dust particles. *Science*, 333(6046), 1121–1125. <https://doi.org/10.1126/science.1207794>
- Ohtake, M., Matsunaga, T., Yokota, Y., Yamamoto, S., Ogawa, Y., Morota, T., et al. (2010). Deriving the absolute reflectance of lunar surface using SELENE (Kaguya) multiband imager data. *Space Science Reviews*, 154(1–4), 57–77. <https://doi.org/10.1007/s11214-010-9689-0>
- Paige, D. A., Foote, M. C., Greenhagen, B. T., Schofield, J. T., Calcutt, S., Vasavada, A. R., et al. (2009). The lunar reconnaissance orbiter diviner lunar radiometer experiment. *Space Science Reviews*, 150(1–4), 125–160. <https://doi.org/10.1007/s11214-009-9529-2>
- Pieters, C. M., Boardman, J., Buratti, B., Chatterjee, A., Clark, R., Glavich, T., et al. (2009). The Moon mineralogy mapper (M<sup>3</sup>) on Chandrayaan-1. *Current Science*, 500–505.
- Pieters, C. M., Ammannito, E., Blewett, D. T., Denevi, B. W., De Sanctis, M. C., Gaffey, M. J., et al. (2012). Distinctive space weathering on Vesta from regolith mixing processes. *Nature*, 491(7422), 79–82. <https://doi.org/10.1038/nature11534>
- Pieters, C. M., Fischer, E. M., Rode, O., & Basu, A. (1993). Optical effects of space weathering: The role of the finest fraction. *Journal of Geophysical Research*, 98(E11), 20817–20824. <https://doi.org/10.1029/93je02467>
- Pieters, C. M., & Noble, S. K. (2016). Space weathering on airless bodies. *Journal of Geophysical Research: Planets*, 121(10), 1865–1884. <https://doi.org/10.1002/2016je005128>
- Pieters, C. M., Rode, O. D., Fisher, E. M., & Basu, A. (1994). Lunar space weathering and the optical properties of lunar regolith. *Astronomicheskii Vestnik*, 28(4–5), 109–119.
- Pieters, C. M., Taylor, L. A., Noble, S. K., Keller, L. P., Hapke, B., Morris, R. V., et al. (2000). Space weathering on airless bodies: Resolving a mystery with lunar samples. *Meteoritics & Planetary Sciences*, 35(5), 1101–1107. <https://doi.org/10.1111/j.1945-5100.2000.tb01496.x>
- Reitze, M. P., Weber, I., Morlok, A., Hiesinger, H., Bauch, K. E., Stojic, A. N., & Helbert, J. (2021). Mid-infrared spectroscopy of Anorthosite samples from near Manicouagan Crater, Canada, as analogue for remote sensing of mercury and other terrestrial solar system objects. *Journal of Geophysical Research: Planets*, 126(8), e2021JE006832. <https://doi.org/10.1029/2021je006832>
- Ruff, S. W., Christensen, P. R., Barbera, P. W., & Anderson, D. L. (1997). Quantitative thermal emission spectroscopy of minerals: A laboratory technique for measurement and calibration. *Journal of Geophysical Research*, 102(B7), 14899–14913. <https://doi.org/10.1029/97JB00593>
- Salisbury, J. W., Basu, A., & Fischer, E. M. (1997). Thermal infrared spectra of lunar soils. *Icarus*, 130(1), 125–139. <https://doi.org/10.1006/icar.1997.5809>
- Salisbury, J. W., Murcray, D. G., Williams, W. J., & Blatherwick, R. D. (1995). Thermal infrared spectra of the Moon. *Icarus*, 115(1), 181–190. <https://doi.org/10.1006/icar.1995.1087>
- Sasaki, S., Nakamura, K., Hamabe, Y., Kurahashi, E., & Hiroi, T. (2001). Production of iron nanoparticles by laser irradiation in a simulation of lunar-like space weathering. *Nature*, 410(6828), 555–557. <https://doi.org/10.1038/35069013>
- Shirley, K. A., & Glotch, T. D. (2019). Particle size effects on mid-infrared spectra of lunar analog minerals in a simulated lunar environment. *Journal of Geophysical Research: Planets*, 124(4), 970–988. <https://doi.org/10.1029/2018je005533>
- Shirley, K. A., Glotch, T. D., Donaldson, O. K., Trelewicz, J., Yang, Y., & Zhang, H. (2023). Effects of albedo on the MIR emissivity spectra of silicates for lunar comparison [Dataset]. Zenodo. <https://doi.org/10.5281/zenodo.7236130>
- Taylor, L. A., Patchen, A., Taylor, D. H. S., Chambers, J. G., & McKay, D. S. (1996). X-ray digital imaging petrography of lunar mare soils: Modal analyses of minerals and glasses. *Icarus*, 124(2), 500–512. <https://doi.org/10.1006/icar.1996.0226>
- Taylor, L. A., Pieters, C. M., Keller, L. P., Morris, R. V., & McKay, D. S. (2001). Lunar mare soils: Space weathering and the major effects of surface-correlated nanophase Fe. *Journal of Geophysical Research*, 106(E11), 27985–27999. <https://doi.org/10.1029/2000je001402>
- Thomas, I. R., Greenhagen, B. T., Bowles, N. E., Donaldson Hanna, K. L., Temple, J., & Calcutt, S. B. (2012). A new experimental setup for making thermal emission measurements in a simulated lunar environment. *Review of Scientific Instruments*, 83(12), 124502. <https://doi.org/10.1063/1.4769084>
- Thompson, M. S., Zega, T. J., Becerra, P., Keane, J. T., & Byrne, S. (2016). The oxidation state of nanophase Fe particles in lunar soil: Implications for space weathering. *Meteoritics & Planetary Sciences*, 51(6), 1082–1095. <https://doi.org/10.1111/maps.12646>
- Weber, I., Reitze, M. P., Heeger, M., Adolphs, T., Morlok, A., Stojic, A. N., et al. (2021). The effect of excimer laser irradiation on mid-IR spectra of mineral mixtures for remote sensing. *Earth and Planetary Science Letters*, 569, 117072. <https://doi.org/10.1016/j.epsl.2021.117072>
- Wentworth, S. J., Keller, L. P., McKay, D. S., & Morris, R. V. (1999). Space weathering on the Moon: Patina on Apollo 17 samples 75075 and 76015. *Meteoritics & Planetary Sciences*, 34(4), 593–603. <https://doi.org/10.1111/j.1945-5100.1999.tb01366.x>
- Yang, Y., Zhang, H., Wang, Z., Yuan, Y., Li, S., Hsu, W., & Liu, C. (2017). Optical Spectroscopic characterizations of laser irradiated olivine grains. *Astronomy & Astrophysics*, 597, A50. <https://doi.org/10.1051/0004-6361/201629327>
- Yang, Y., Zhang, H., Wang, Z., Yuan, Y., Li, S., Hsu, W., & Liu, C. (2021). Optical Spectroscopic characterizations of laser irradiated olivine grains (Corrigendum). *Astronomy & Astrophysics*, 646, C1. <https://doi.org/10.1051/0004-6361/201629327>